Droplet actuation on superhydrophobic substrates via electric field gradients

Cite as: Appl. Phys. Lett. **114**, 113702 (2019); doi: 10.1063/1.5080241
Submitted: 6 November 2018 · Accepted: 4 March 2019 ·
Published Online: 20 March 2019

View Online Export Citation CrossMark

H. Alex Guo, Shagun Maheshwari, Maya S. Patel, Eeshan C. Bhatt, and Chuan-Hua Chen[a)]

AFFILIATIONS

Department of Mechanical Engineering and Materials Science, Duke University, Durham, North Carolina 27708, USA

[a)]chuanhua.chen@duke.edu

ABSTRACT

A superhydrophobic surface is non-sticking to aqueous droplets due to minimized solid-liquid contact, but the small contact area also poses challenges to droplet maneuvering. This letter reports a technique using electric field gradients to actuate aqueous droplets on superhydrophobic surfaces. A pin-ring electrode pair underneath the insulating superhydrophobic surface is used to generate electric field gradient above the surface, with the field focused around the pin. The non-uniform field operates on the electrostatically induced charges on the droplet, producing an actuation force attracting the droplet toward the pin. The actuation force is proportional to the square of the imposed field as shown in both experiments and simulations. This non-contact actuation technique is effective in electrostatically trapping and translating superhydrophobic droplets, despite the small solid-liquid contact. The pin-ring configuration can be readily extended to a pin array between two parallel lines, which essentially form a stretched ring closing at infinity. The pin array is used to demonstrate individual actuation of two droplets leading to their eventual coalescence.

On a superhydrophobic substrate with a contact angle close to 180°, an aqueous droplet has a minimal liquid-solid contact, giving rise to many special features of the superhydrophobic surface.[1] Although the minimal contact is critical to the high mobility of droplets on superhydrophobic substrates, it also presents a special challenge for droplet actuation because the "non-sticking" superhydrophobic surface cannot exert sufficient force on the droplet. One way to address this challenge is to use magnetic actuation,[2–4] which entails an additive to render the bulk droplet magnetically responsive. Despite the versatility of this technique, the magnetic additive alters (contaminates) the liquid droplets and is undesirable for many applications including most biomedical ones. In this letter, we employ an electric field gradient to actuate superhydrophobic droplets without using any additive to the droplets. Although electrostatic actuation has been applied to superhydrophobic droplets in prior reports,[5–11] our work is distinct in imposing field gradients with a pin-ring electrode configuration that is independent of the superhydrophobic substrate, thus circumventing the complexity of electrode embedment.

The essential components of the electrostatic actuator are shown in Fig. 1. The actuator consists of an insulating superhydrophobic substrate on which an aqueous droplet initially rests, and a pin and a surrounding ring that are both underneath the substrate, as depicted in Fig. 1(a). With the pin at the center of the grounded ring, the electrode pair produces strong electric field gradients, which are responsible for the actuation. The pin is perpendicularly protruded from the plane of the ring electrode to facilitate close contact between the pin and the bottom of the substrate. Otherwise, the protrusion is not essential to the actuation mechanism, and our setup somewhat resembles the coplanar electrode configuration in electrowetting.[12–16] The pin-ring configuration enables versatile actuation of droplets on superhydrophobic surfaces. When the droplet is off-centered with respect to the pin in Fig. 1(b), it experiences an in-plane field gradient. Although the droplet is net neutral, the electrostatic force on the induced charges is stronger on the side closer to the pin. The net force attracts the droplet toward the center. As a consequence, the droplet is trapped around the pin in Fig. 1(c), where the net electrostatic force only has a vertical component, holding the droplet against the substrate. The principle depicted in Fig. 1 is analogous to that of dielectrophoresis[17,18] in that the actuation force arises from electrostatically induced charges on a net-neutral droplet.

The same actuation principle can be extended to the electrostatic actuation of multiple droplets. For this purpose, the pin-ring configuration in Fig. 1(a) needs to be modified to accommodate a pin array. One possibility is shown in Fig. 1(d) with the ring replaced by two parallel lines, which essentially form a stretched ring closing at infinity. In between the parallel electrodes, an array of pins can be positioned for

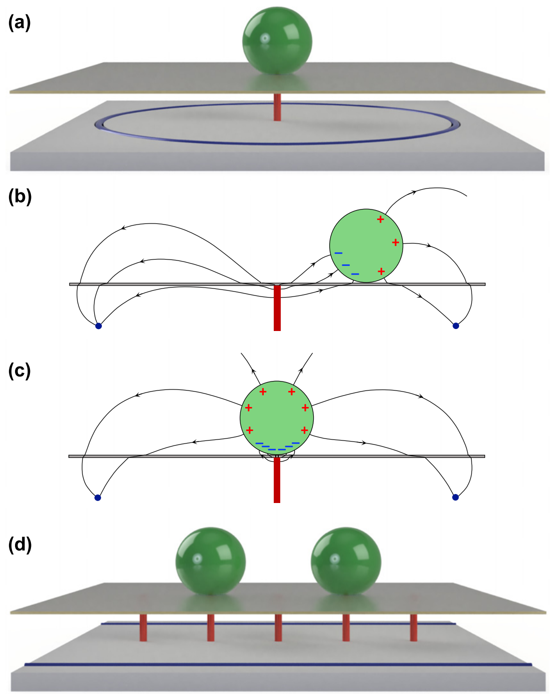

FIG. 1. The electrostatic actuation of an aqueous droplet on a superhydrophobic substrate: (a) The pin-ring electrode configuration traps a droplet around the pin. (b) The off-centered droplet experiences an in-plane trapping force toward the center. (c) The droplet is trapped at the center, because any perturbation to this symmetric arrangement will produce an in-plane restoring force toward the center. (d) A pin array between two parallel line electrodes can actuate multiple droplets. In (a) and (d), the top plate is the superhydrophobic substrate, and the bottom plate is an insulator supporting the electrodes.

individual control of multiple droplets. Below, we will primarily use the pin-ring configuration to study the actuation of a single droplet and will additionally use the pin array between parallel lines to demonstrate the actuation of multiple droplets. Our technique is, therefore, applicable to a variety of interfacial systems[1,4,19,20] that require the control of superhydrophobic droplets individually[3,7,8] or collectively.[5,10,11]

In our experiments, the superhydrophobic substrate is made of a thin glass coverslip (Electron Microscopy Sci. 63751) coated with a superhydrophobic spray paint (Cytonix WX2100). The #0 coverslip has a thickness of $100 \pm 20\,\mu$m. The coverslip is coated using a procedure detailed in the supplementary material in order to prevent micron-scale cracks that degrade the superhydrophobicity. On the coated coverslip, the advancing and receding contact angles for water are $162^\circ \pm 2^\circ$ and $150^\circ \pm 13^\circ$, respectively. The droplet is deposited by a pipette (Eppendorf 022471902) and monitored with a camera (Phantom V710) through a long-distance microscope (Infinity K2 with a CF-1 or CF-2 lens).

The field gradients are produced by electrifying the pin-ring electrode pair with a high-voltage amplifier (Trek 610E) and a waveform generator (Agilent 33220A). The pin and ring are both made of bare copper wires with a diameter of 0.25 mm (Arcor 30AWG). The diameter of the ring electrode is 12 ± 0.5 mm. The pin electrode is at the center of the ring and perpendicularly protrudes from the plane of the ring electrode by 1.5 ± 0.3 mm. When the pin-ring pair needs to be translated (to translate the trapped droplet along with it), both electrodes are attached to a linear micrometer stage (Edmund 37-980). When the entire setup (substrate and the electrodes) needs to be tilted, a goniometer (Edmund NT55-838) is used to incrementally change the tilt angle.

The electrostatic actuation is demonstrated in Fig. 2 (Multimedia view), where a water droplet is trapped and translated on a superhydrophobic substrate. In Fig. 2(a), a deionized water droplet is initially deposited on the superhydrophobic surface, approximately 1 mm away from the pin electrode. The droplet is attracted toward the pin when an alternating current (AC) field is applied on the pin-ring pair, with a root-mean-square voltage $V_{rms} = 2.8$ kV and a frequency $f = 500$ Hz. The trapping process is very quick, taking less than 50 ms in Fig. 2(a). Since the droplet is deformable, the trapping process is more complicated than that depicted in Fig. 1. The droplet movement is accompanied by the asymmetric deformation of the droplet in the non-uniform field, with stronger deformation (and smaller apparent contact angle) closer to the pin. In Fig. 2(b), a trapped droplet tracks the pin-ring pair, which is translated underneath the superhydrophobic surface. The droplet movement lags the electrode movement slightly because the translating force is created by a slight off-center displacement of the droplet with respect to the electrode pair. This in-plane translating force is needed to overcome the hindering force from the superhydrophobic surface. Note that the translation experiment implies a two-step process in a typical scenario: a droplet is first attracted by the pin electrode as soon as the field is turned on, and the trapped droplet is then translated by the moving pin-ring pair.

Throughout this paper, we use a fixed AC frequency of 500 Hz, which yields consistent trapping performance. At this frequency, the AC field induces a barely perceptible oscillation of the droplet shape; see the image at 14.3 ms in Fig. 2(a). The AC field also prevents any

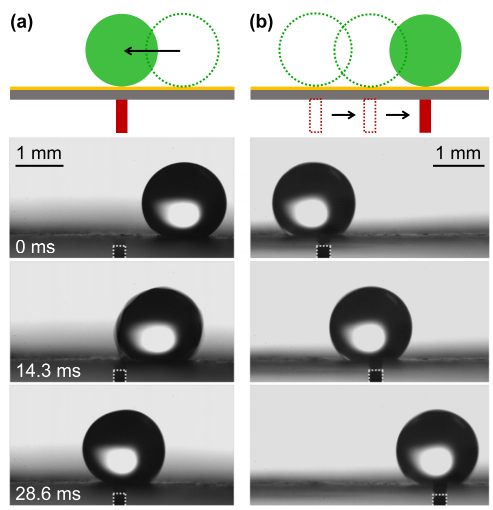

FIG. 2. The electrostatic actuation of a deionized water droplet on a superhydrophobic surface: (a) Trapping of an off-centered droplet; (b) translation of a trapped droplet. The AC field ($V_{rms} = 2.8$ kV, $f = 500$ Hz) is applied between a pin and a ring. The 12 mm-diameter ring is centered around the pin (white dashed line) but outside the field of view. Multimedia views: https://doi.org/10.1063/1.5080241.1; https://doi.org/10.1063/1.5080241.2

net translation of the droplet in the presence of a net charge, which may arise from interfacial charge separations.[21–23] The intermediate frequency of 500 Hz is chosen to avoid large-amplitude oscillation of the droplet at lower frequencies ($\lesssim$10 Hz). At the same time, this frequency is well below the high-frequency regime ($\gtrsim$ 100 kHz, see below) in which the deionized water droplet can no longer be idealized as a conductor.

To quantitatively study the actuation mechanism, we measure the actuation force on the droplet by tilting the superhydrophobic substrate in Fig. 3. At a given voltage, the entire setup including the substrate is tilted at an increasing angle, until gravitational force along the titled substrate overcomes the trapping force. The critical slide-off angle α indicates the strength of trapping, which is a function of the applied voltage V_{rms}. The experimental procedure to identify the critical angle α is detailed in Sec. S1 in the supplementary material. In Fig. 3(a), droplet images are captured at incipient slide-off. At high voltages, the droplet deformation leads to a strong asymmetry and a much reduced apparent contact angle, a reduction that is similarly observed in electrowetting.[24,25]

In Fig. 3(b), the sliding angle is converted into the gravitational force component along the substrate

$$F_g = mg \sin\alpha, \tag{1}$$

where m is the droplet mass, and g is the gravitational constant. To explain the quadratic relationship between F_g and V_{rms}, we note that the sliding force F_g is balanced by the electrostatic trapping force F_e exerted by the nonuniform field. Since the electrostatic actuation is based on induced charges, the trapping force is expected to be proportional to voltage squared

$$F_e = \lambda_e V_{\mathrm{rms}}^2, \tag{2}$$

where the coefficient λ_e accounts for the geometrical configuration including the pin-ring electrodes, the dielectric substrate, the droplet radius, shape, and displacement. Note that the shape of the deformable droplet is a function of the Maxwell stress, which typically depends on V_{rms}.

To further support the simple model in Eq. (2), we estimate λ_e through numerical simulation of the electrostatic trapping. The water droplet is approximated as a conductor with instant charge relaxation. For deionized water, the conductivity $\sigma \sim 10^{-4}$ S/m and the permittivity $\epsilon \sim 10^{-9}$ F/m, so our frequency is well below the limit of $\sigma/\epsilon \sim 10^5$ Hz set by the charge relaxation process.[17,24] Further, the droplet is simplified as a rigid sphere (with a contact angle of 180°) to avoid complications arising from electromechanical coupling. Under these assumptions, the electric field distribution around the conducting droplet and the insulating substrate can be easily calculated (COMSOL version 4.2). Except for the simplified droplet shape, other geometrical parameters in the setup are faithfully reproduced in the three-dimensional simulations. The net force on the droplet is integrated from the Maxwell stress distribution on the droplet surface.[18,24] For a conducting droplet, the electric field only exists on the air side and is normal to the spherical droplet surface. The in-plane component of the electric force F_x is given by a surface integral

$$F_x = \oint \frac{1}{2}\varepsilon_0 E^2 n_x dA = -\lambda_e V^2, \tag{3}$$

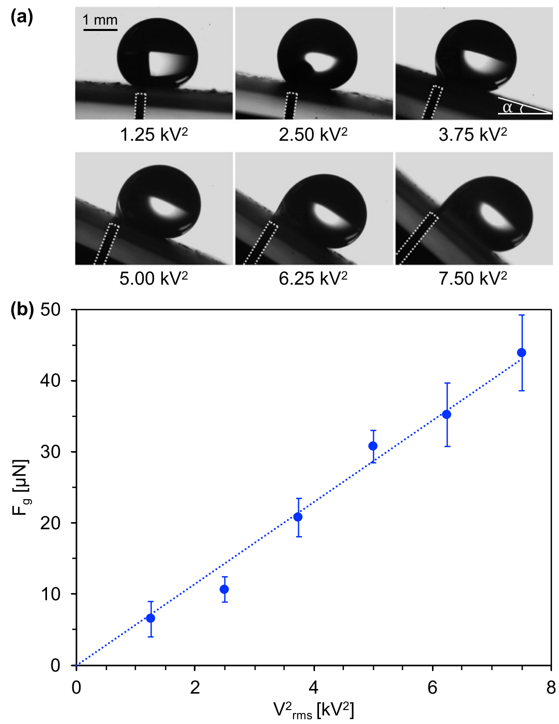

FIG. 3. The electrostatic trapping force measured by the slide-off angle α: (a) Images of the droplet captured right before the slide-off by gravity, which points downward. The 12 mm-diameter ring is centered around the pin (white dashed line) but outside the field of view. AC frequency: $f = 500$ Hz; droplet volume: $\Omega = 7.1\,\mu$l. (b) The sliding force, $F_g = mg\sin\alpha$, as a function of the applied voltage squared, V_{rms}^2. A linear fitting with $F_g = \hat{\lambda}_e V_{\mathrm{rms}}^2$ yields an actuation coefficient of $\hat{\lambda}_e = 5.7\ \mu\mathrm{N/kV}^2$ for $\Omega = 7.1\,\mu$l.

where x is the in-plane displacement defined in the inset of Fig. 4(a), ε_0 is the air permittivity, E is the local electric field on the air side, n_x is the x-component of the surface normal, dA is the differential surface area, and V is the (constant) applied voltage. The trapping force is toward the origin; therefore, the negative sign in Eq. (3).

In Fig. 4(a), the in-plane actuation force toward the center is calculated as a function of the off-center displacement of the droplet. As depicted in the inset Fig. 4(a), the displacement x gives rise to the in-plane trapping force (to restore the symmetry). Assuming the droplet to be perfectly spherical, the force peaks when the displacement approximately equals a pin diameter (0.25 mm). Further displacement leads to a reduction in the in-plane force because the field is weaker away from the pin. The maximum value of λ_e is defined as the actuation coefficient $\hat{\lambda}_e$. For a droplet volume of $\Omega = 7.1\,\mu$l, the actuation coefficient is $\hat{\lambda}_e = 10.0\ \mu\mathrm{N/kV}^2$ in Fig. 4. This value is reasonably close to the measured value of $\hat{\lambda}_e = 5.7\ \mu\mathrm{N/kV}^2$ in Fig. 3(b). In Fig. 4(b), the actuation coefficient $\hat{\lambda}_e$ is simulated for a range of droplet volume Ω. When Ω increases by 100×, $\hat{\lambda}_e$ increases by merely 2×. The weak dependence of the actuation coefficient on the droplet volume is supported by experimental measurements at 4.0 μl versus 7.1 μl, shown in Fig. S1 in the supplementary material.

In our setup, the pin plays a dominant geometrical role. The pin diameter is much smaller than the droplet diameter, which is in turn much smaller than the ring diameter. Given a thin enough

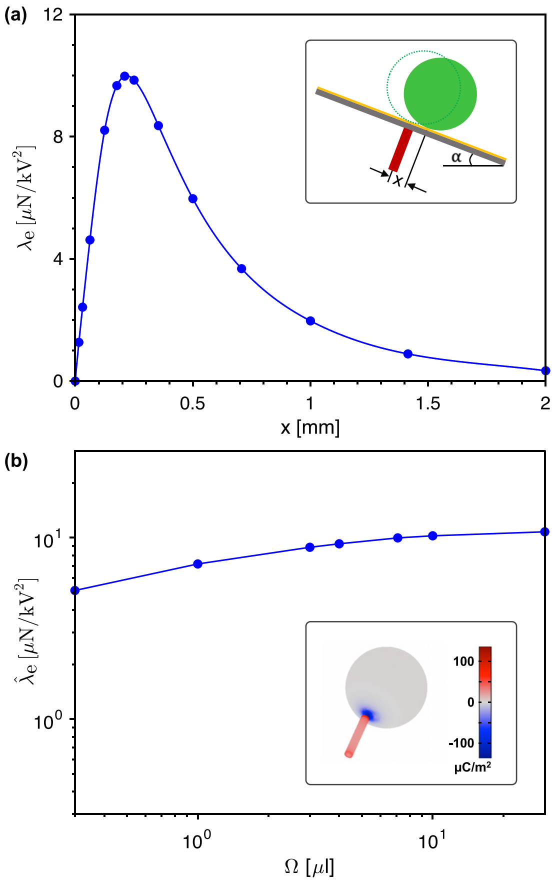

FIG. 4. Simulations of the coefficient λ_e for the in-plane electrostatic force: (a) The simulated λ_e versus the off-center displacement x. For a droplet volume of $\Omega = 7.1\ \mu$l, the actuation coefficient is $\hat{\lambda}_e = 10.0\ \mu\text{N/kV}^2$, which is the maximum value of $\lambda_e(x)$. Inset: At a tilt angle α, the droplet (idealized as spherical) is displaced by an off-center distance x. (b) The actuation coefficient $\hat{\lambda}_e$ versus droplet volume Ω. The volume dependence is weak, especially when the droplet diameter (1.8 mm at 3 μl) is much larger than the pin diameter (0.25 mm). Inset: The surface charge distribution on the droplet (at a constant voltage of 1 kV) is concentrated around the pin. The substrate is omitted for clarity.

superhydrophobic substrate, the pin will focus the electric field around itself. The focusing effect is apparent in the inset of Fig. 4(b), where the induced charges on the droplet surface are concentrated around the area opposing the pin. The focusing effect is also corroborated by Figs. 4(a) and S2, where the actuation force at each volume peaks when the droplet is displaced by approximately a pin diameter.

The dominating role of the pin in shaping the electric field explains the insensitivity of the actuation coefficient $\hat{\lambda}_e$ to droplet volume in Fig. 4(b). The dominance may further explain the paradoxical insensitivity of $\hat{\lambda}_e$ to droplet deformation in Fig. 3. On one hand, since the droplet shape varies with the electric field, $\hat{\lambda}_e$ which absorbs the geometrical factors is expected to be dependent on the voltage. On the other hand, the electric field is highly concentrated around the pin, so only a small fraction of the droplet surface area matters in terms of electrostatic force generation. As a result, $\hat{\lambda}_e$ is not very sensitive to droplet deformation in Fig. 3. The quadratic relationship in Eq. (2) provides a simple design guideline, which is particularly useful given the insensitivity of the prefactor $\hat{\lambda}_e$ to droplet volume and applied voltage.

Given the dominant geometrical role played by the pin, our electrostatic actuation technique retains essentially the same features when the ring electrode is substituted with parallel lines, as sketched in Fig. 1(d). Since the electric field focuses around individual pins, an array of adequately spaced pin electrodes can more or less function independently from each other. This independence will greatly facilitate scale-up efforts in applications that require a complex electrode arrangement (as in digital microfluidics[20]). Using the pin array between parallel lines, two droplets are individually actuated toward their eventual coalescence in Fig. 5 (Multimedia view). A linear array of five pins is positioned underneath a superhydrophobic substrate, as shown in Fig. 5(a). The adjacent pins are 1 mm apart, all centered between two parallel ground electrodes, as sketched in Fig. 1(d). The parallel electrodes are separated by 12 ± 1 mm (same as the ring diameter). The pins protrude 3 ± 0.5 mm above the parallel electrodes. In Fig. 5(b), two droplets are placed on top of the plate, initially above pins 1 and 5, which are electrified at identical AC voltage ($V_{\text{rms}} = 2.5$ kV, $f = 500$ Hz). The rest of the pins are floating. In Fig. 5(c), the same voltage is applied to pins 2 and 4 with the other pins floating, so as to move the droplets toward each other. In Fig. 5(d), the same voltage is applied on pin 3 alone, attracting both droplets toward the center pin and coalesce above it.

Some limitations of our present work are worth noting. (i) The commercially available superhydrophobic coating is sufficient for most practical applications, but not ideal for fundamental studies. Substrates prepared from different spray cans may exhibit a 5° to 10° variation in the contact angle, making repeated measurements difficult. The same coating made of a polymer-nanoparticle composite shows degradation over extended exposure to strong electric fields. Kilovolt-level voltages are needed to penetrate the non-conducting substrate, but may ionize air and degrade the polymeric coating. (ii) Our measurement of trapping force by gravitational slide-off only works over a limited parametric range. Although we have verified electrostatic trapping for droplet volume ranging from 0.3 μl to 30 μl (the full range of applicability is likely larger), the actuation coefficient $\hat{\lambda}_e$

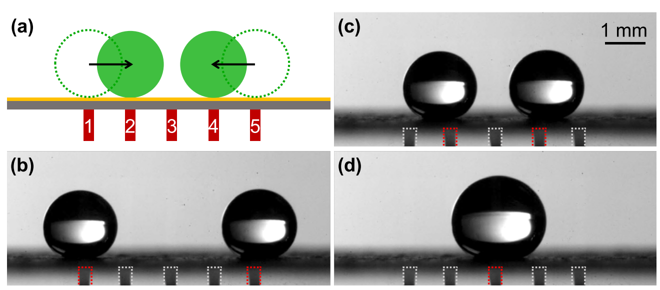

FIG. 5. Sequential actuation of two droplets leading up to their coalescence: (a) A linear array of pins is positioned underneath a superhydrophobic substrate, between two grounded electrode lines (not visible here). (b) Two droplets are initially placed above pins 1 and 5 that are electrified (red dashed lines) at an identical AC voltage. The rest of the pins are floating (white dashed lines). (c) Pins 2 and 4 are electrified, moving the droplets toward each other. (d) Pin 3 alone is electrified, attracting both droplets to coalesce above this center pin. Multimedia view: https://doi.org/10.1063/1.5080241.3

can only be reliably measured at an intermediate volume—the smaller droplets are disproportionally affected by the hysteresis of the substrate, while the larger droplets are strongly deformed by gravity. As a further complication, the pins cannot be cut with a perfectly circular cross section, making it challenging to experimentally vary the pin diameter. For consistent measurements in Figs. 3 and S1, we used the same pin and ring electrodes. (iii) In addition to idealizing the pin shape, the numerical model simplifies the droplet as a rigid sphere. These two assumptions are probably responsible for the discrepancy between simulated and measured actuation coefficient $\hat{\lambda}_e$. Unfortunately, any contact angle below 180° introduces electromechanical divergence at the triple contact line. (The divergence is a well-documented difficulty[24,26,27] beyond the scope of this letter.) The rigid sphere approximation excludes any electromechanical deformation in the simulation although strong deformation is observed at high fields. Consistent with the 180° assumption, we have ignored the hysteresis force on the superhydrophobic surface, measured as $4.9 \pm 1.1\,\mu$N, which is small compared to most of the data points in Fig. 3(b).

In conclusion, we have demonstrated an electrostatic mechanism to actuate aqueous droplets on a superhydrophobic substrate. The actuation force is produced by a pin-ring electrode pair underneath the substrate. The pin focuses electric field around itself, and the non-uniform field exerts a net force on charges induced on the droplet, attracting the droplet toward the pin. The ring electrode can be replaced by two parallel lines, enabling the incorporation of a pin array for the actuation of multiple droplets. Our electrostatic actuation technique retains the high mobility of superhydrophobic droplets while avoiding direct contact between the actuating electrodes and the droplets.

See supplementary material for detailed experimental procedures and additional data on volume effect.

This work was supported by the National Science Foundation Research Triangle MRSEC (DMR-1121107). E.C.B. was supported by the Pratt Fellows Program at Duke University.

REFERENCES

1. P.-G. de Gennes, F. Brochard-Wyart, and D. Quéré, *Capillarity and Wetting Phenomena* (Springer, 2004).
2. Y. Zhao, J. Fang, H. Wang, X. Wang, and T. Lin, Adv. Mater. **22**, 707 (2010).
3. L. Mats, F. Logue, and R. D. Oleschuk, Anal. Chem. **88**, 9486 (2016).
4. G. Huang, M. Li, Q. Yang, Y. Li, H. Liu, H. Yang, and F. Xu, ACS Appl. Mater. Interfaces **9**, 1155 (2017).
5. M. Washizu, IEEE Trans. Ind. Appl. **34**, 732 (1998).
6. K. Takeda, A. Nakajima, Y. Murata, K. Hashimoto, and T. Watanabe, Jpn. J. Appl. Phys., Part 1 **41**, 287 (2002).
7. S. L. S. Freire and B. Tanner, Langmuir **29**, 9024 (2013).
8. S. Lee, S. Lee, D. Kim, J. Seo, C. Mahata, H. Hwang, H. Algadi, S. Al-Sayari, Y. Chae, and T. Lee, RSC Adv. **5**, 5754 (2015).
9. D. J. Preston, A. Anders, B. Barabadi, E. Tio, Y. Zhu, D. A. Dai, and E. N. Wang, Appl. Phys. Lett. **109**, 244102 (2016).
10. X. Yan, J. Li, L. Li, Z. Huang, F. Wang, and Y. Wei, Appl. Phys. Lett. **109**, 161601 (2016).
11. B. Traipattanakul, C. Tso, and C. Y. Chao, Int. J. Heat Mass Transfer **128**, 550 (2019).
12. U.-C. Yi and C.-J. Kim, J. Micromech. Microeng. **16**, 2053 (2006).
13. A. Vasudev and J. Zhe, Appl. Phys. Lett. **93**, 103503 (2008).
14. J.-T. Cheng and C.-L. Chen, Nanoscale Microscale Thermophys. Eng. **14**, 63 (2010).
15. G. McHale, C. V. Brown, M. I. Newton, G. G. Wells, and N. Sampara, Phys. Rev. Lett. **107**, 186101 (2011).
16. D. 't Mannetje, S. Ghosh, R. Lagraauw, S. Otten, A. Pit, C. Berendsen, J. Zeegers, D. van den Ende, and F. Mugele, Nat. Commun. **5**, 3559 (2014).
17. H. A. Pohl, *Dielectrophoresis* (Cambridge University Press, 1978).
18. R. Pethig, *Dielectrophoresis* (Wiley, 2017).
19. T. M. Squires and S. R. Quake, Rev. Mod. Phys. **77**, 977 (2005).
20. R. B. Fair, Microfluid. Nanofluid. **3**, 245 (2007).
21. R. J. Hunter, *Zeta Potential in Colloid Science* (Academic Press, 1981).
22. D. Choi, H. Lee, D. J. Im, I. S. Kang, G. Lim, D. S. Kim, and K. H. Kang, Sci. Rep. **3**, 2037 (2013).
23. N. Miljkovic, D. J. Preston, R. Enright, and E. N. Wang, Nat. Commun. **4**, 2517 (2013).
24. F. Mugele and J.-C. Baret, J. Phys. Condens. Matter **17**, R705 (2005).
25. T. B. Jones, Langmuir **18**, 4437 (2002).
26. M. Vallet, M. Vallade, and B. Berge, Eur. Phys. J. B **11**, 583 (1999).
27. K. H. Kang, Langmuir **18**, 10318 (2002).